Measurement and Global Analysis of the Absorbance Changes in the Photocycle of the Photoactive Yellow Protein from *Ectothiorhodospira halophila*

W. D. Hoff,* I. H. M. van Stokkum,‡ H. J. van Ramesdonk,§ M. E. van Brederode,* A. M. Brouwer,§ J. C. Fitch,¶ T. E. Meyer,¶ R. van Grondelle,‡ and K. J. Hellingwerf*

*Department of Microbiology, E.C. Slater Institute, BioCentrum Amsterdam, University of Amsterdam; ‡Faculty of Physics and Astronomy, Free University, Amsterdam; §Laboratory of Organic Chemistry, University of Amsterdam, The Netherlands; ¶Department of Biochemistry, University of Arizona, Tucson, Arizona, USA

ABSTRACT The photocycle of the photoactive yellow protein (PYP) from *Ectothiorhodospira halophila* was examined by time-resolved difference absorption spectroscopy in the wavelength range of 300–600 nm. Both time-gated spectra and single wavelength traces were measured. Global analysis of the data established that in the time domain between 5 ns and 2 s only two intermediates are involved in the room temperature photocycle of PYP, as has been proposed before (Meyer T. E., E. Yakali, M. A. Cusanovich, and G. Tollin. 1987. *Biochemistry.* 26:418–423; Meyer, T. E., G. Tollin, T. P. Causgrove, P. Cheng, and R. E. Blankenship. 1991. *Biophys. J.* 59:988–991). The first, red-shifted intermediate decays biexponentially (60% with τ = 0.25 ms and 40% with τ = 1.2 ms) to a blue-shifted intermediate. The last step of the photocycle is the biexponential (93% with τ = 0.15 s and 7% with τ = 2.0 s) recovery to the ground state of the protein. Reconstruction of the absolute spectra of these photointermediates yielded absorbance maxima of about 465 and 355 nm for the red- and blue-shifted intermediate with an ϵ_{max} at about 50% and 40% relative to the ϵ_{max} of the ground state. The quantitative analysis of the photocycle in PYP described here paves the way to a detailed biophysical analysis of the processes occurring in this photoreceptor molecule.

INTRODUCTION

A number of halophilic purple phototrophic organisms contain a water-soluble, photoactive yellow protein (PYP) (Meyer, 1985; Meyer et al., 1990; Hoff et al., 1994). The PYP isolated from *Ectothiorhodospira halophila* has been examined in some detail with respect to its (photo)physical properties. The protein has an absorbance maximum at 446 nm and an ϵ_{446} of 45.5 mM^{-1}cm^{-1} (Meyer, 1985; Meyer et al., 1989). Determination of the crystal structure of PYP revealed that it belongs to the β-clam family and therefore is the first and only non-eukaryotic protein known to have this type of structure (McRee et al., 1989). In addition, it has been demonstrated that the protein is photoactive: after absorption of a photon by its broad absorbance band at 446 nm, the protein engages in a cyclic series of dark reactions (Meyer et al., 1987). Recently, evidence has been obtained indicating that PYP in *E. halophila* functions as the photoreceptor for a negative phototactic response (Sprenger et al., 1993).

It has been proposed that the PYP photocycle involves two sequentially populated intermediates that show monoexponential behavior. Specifically, the first photocycle intermediate is bathochromically shifted and is formed within 10 ns

(not time resolved; Meyer et al., 1989). This intermediate is transformed into a hypsochromically shifted intermediate with a rate constant between 2000 and 7500 s^{-1}. Subsequently, this blue-shifted state of the protein recovers its yellow color with a rate constant of about 2 s^{-1} (Meyer et al., 1987; Meyer et al., 1991). It has been reported that this recovery process involves a second, related blue-shifted intermediate (Meyer et al., 1987). However, the existence of this intermediate is uncertain (compare Meyer et al., 1987, 1989, 1991, and 1993), and it is possible that various preparations of PYP display different behavior caused by an unknown source of heterogeneity, a topic that also bears on the results reported here. These measurements were performed with a single-wavelength experimental setup in a wavelength range of 360–540 nm (at 30 wavelengths) with a time resolution of 1 μs. A rigorous model-based global analysis of the absorbance changes occurring during the PYP photocycle has not yet been reported.

In a number of ways PYP resembles the bacterial rhodopsins. These retinal proteins can be divided into two groups, sensory rhodopsin I, (slow rhodopsin) and sensory rhodopsin II, (phoborhodopsin) that perform a photosensory function (Spudich and Bogomolni, 1988), and on the other hand bacteriorhodopsin (bR) and halorhodopsin that perform an ion-pumping function (Oesterhelt and Tittor, 1989). Because PYP is a photoreceptor it functionally resembles the sensory rhodopsins, especially sensory rhodopsin II, which also functions as a repellent photoreceptor and has an absorbance maximum of 487 nm. That PYP functions as a photoreceptor is supported by indirect evidence for the involvement of a large conformational change in the protein

during the photocycle of PYP, but the conformation of the blue-shifted state of the protein has not yet been resolved (Meyer et al., 1989).

In addition, the photophysics of PYP and the rhodopsins have many characteristics in common. First, the rate constants and the direction and size of the shifts in absorbance maximum observed in the photocycle are similar to those reported for a number of Halobacterial retinal proteins (Meyer et al., 1987; Stavenga et al., 1991). The spectral and kinetic characteristics of the rhodopsins, and especially bR, have been studied extensively using a number of spectroscopic and data analysis techniques (Birge, 1990; Hessling et al., 1993; Lanyi, 1992; Mathies et al., 1991; Zimanyi and Lanyi, 1993). However, no consensus has been reached yet on the exact photocycle scheme in bR. An important reason for this is that the absorbance spectra of the different intermediates strongly overlap (both spectrally and temporally), a problem that also occurs in the photocycle of PYP. The flash-induced absorbance changes in sensory rhodopsin I have been analyzed assuming a unidirectional, unbranched reaction scheme (Bogomolni and Spudich, 1987).

A second area of parallels between the photochemistry of PYP and the rhodopsins is found in their low temperature absorbance and fluorescence characteristics (Hoff et al., 1992). At 77 K a bathointermediate of PYP is trapped, indicating that the photocycle can be blocked after its first step. In addition, a strongly fluorescent intermediate is formed in parallel with this red-shifted intermediate. This situation closely resembles that in bR at 77 K. The third photophysical characteristic shared by PYP and the rhodopsins is the presence of a light-dependent branching reaction in the photocycle of these proteins (Miller et al., 1993, and references therein). In this branching reaction the blue-shifted intermediate, which thermally decays slowly to the ground state, is converted to the ground state at a strongly increased rate (in comparison with the thermal reaction) after the absorption of a photon. Both the initial and the branching photoreaction in PYP have a high quantum yield (Meyer et al., 1989; Miller et al., 1993). A similar situation exists in the bacterial rhodopsins (Birge, 1990). Additional similarities are observed in the fluorescence properties of the primary excited state of these proteins. The fluorescence quantum yield of PYP was determined to be near $2.5 * 10^{-3}$ (Meyer et al., 1991; Hoff et al., 1992), whereas 90% of the emission occurs with a lifetime of 12 ps (Meyer et al., 1991). In the case of bR the quantum yield of fluorescence is approximately 10-fold lower (Lewis et al., 1976). Maximal fluorescence emission of PYP occurs at 495 nm, and maximal fluorescence excitation at 457 nm (Meyer et al., 1991; Hoff et al., 1992). A discrepancy between the absorbance maximum and the fluorescence excitation maximum has been observed in bR also (Govindjee et al., 1978).

In complete contrast with the photochemical similarities between PYP and the rhodopsins the two types of protein lack all structural resemblance. Whereas PYP is completely composed of β-strands (a β-clam, see above), the rhodopsins only contain α-helices. PYP shows no obvious sequence

similarity to either rhodopsins or other β-clam proteins (Van Beeumen et al., 1993). Also the structures of the chromophoric groups involved are strikingly different. Whereas the rhodopsins all contain a retinal molecule linked to the apoprotein via a Schiff base, the chromophore in PYP is attached to the protein via a disulfide bridge to cystein 69 and has a molecular weight of 147 Da, different from that of retinal (Van Beeumen et al., 1993). This leads to a paradoxical situation: how can two structurally very different proteins display the same photochemical activities?

In this paper we describe time-resolved multichannel and single-wavelength difference absorbance measurements in the wavelength range of 300–600 nm. Because the multichannel measurements have a high spectral resolution and the single wavelength measurements have a high temporal resolution, these two datasets complement each other. With these data we have examined the spectral and kinetic characteristics of the PYP photocycle using a global analysis approach to obtain a detailed description of this process. We have determined the rank of the matrix formed by concatenating either the time-gated spectra or the traces measured at different wavelengths. In both cases a rank of 2 was found, which demonstrates quantitatively that only two photointermediates are involved in the photocycle of PYP from *E. halophila* in the ns-to-s time domain. We have analyzed the data globally using a temporal, kinetic model as well as a spectral and spectrotemporal model. Under certain assumptions, the results of the global analysis allow the reconstruction of the absolute absorbance spectra of the two intermediates. The kinetics of the photocycle were found to be more complex than expected on the basis of the model that has been proposed previously. With these results, a quantitative description of the photocycle of this eubacterial photoreceptor protein and its physiological activity becomes possible.

MATERIALS AND METHODS

Experimental

Sample preparation

PYP from *E. halophila* was isolated according to Meyer (1985) with some modifications. The cells were either grown in batch in a complex medium (Meyer, 1985) or in a continuous culturing system in a mineral medium described by Imhoff and Trüper (1977; supplemented with 0.1 M carbonate buffer (pH 9.0) and without yeast extract and vitamin solution). The cells were harvested and resuspended at a concentration of about 300 g (wet weight)/l, disrupted, and ultracentrifuged. After dialysis the supernatant was applied to a DEAE DE52 cellulose column (Whatman Biosystems, Maidstone, UK) at pH 8.0. As expected, PYP eluted as the first chromophoric protein at ~150 mM NaCl. After repeating this chromatography, the protein was concentrated, freeze-dried, and applied on a size exclusion column (either sephacryl S100 HR or superose 12 (Pharmacia, Uppsala, Sweden) on an FPLC system). The major part of the PYP eluting from the size exclusion column had a purity index (absorbance at 280 nm divided by absorbance at 446 nm) of 0.50, indicating that the protein was pure. About 15 mg of PYP was recovered per kg of cells (wet weight). The homogeneity of the sample was confirmed by electrospray mass spectrometry; one of the samples used in this study was from the same batch used to obtain the electrospray mass spectrum in Fig. 6 of Van Beeumen et al. (1993). The protein was freeze-dried and dissolved in 10 mM Tris-HCl (pH 7.5) to an

optical density of about 1 at 446 nm and was studied in 3-ml quartz fluorescence cuvettes. In this study PYP was used from two independent protein isolations from two independently grown batches of cells.

Time-resolved multichannel absorbance measurements

Laser flashes at 355 nm of 8 ns (full width at half maximum) were obtained from an Nd-YAG laser GCR-3 (Quanta-Ray/Spectra Physics, Mountain View, CA) using an NLO KD*P (Quanta-Ray/Spectra Physics) harmonic generator crystal. These laser pulses were used to pump a PDL-3 dye laser (Quanta-Ray/Spectra Physics) using Coumarin 440 as a dye to obtain flashes at 446 nm. In some cases a diffusor was used to eliminate hot spots in the laser beam. The flash frequency used was 0.2 Hz, with an energy of 10 mJ/flash. The measuring light was provided by a high-pressure Xe lamp LAX1450 with power supply SV1450 (Müller, Moosinning, Germany). This light reached the sample through a 1×2-mm hole in the sample holder right after and perpendicular to the surface of the cuvette where the laser flash was applied. Changes in the absorption of the sample were detected by collecting the measuring light with an optical fiber, which was fed into a Jarrel-Ash (Allied Analytical Systems, Waltham, MA) monospec 27 model 1234 spectrograph in which the light was dispersed by a grating (150 grooves/mm) onto a gated MCP-intensified diode array detector (EG&G (Princeton, NJ) 1421G, 25 mm, 1024 diodes) with a bandwidth of 7 nm for ns experiments and 2.4 nm for μs-to-s experiments. Excitation of the PYP sample by the measuring light from the Xe lamp was reduced to a minimum by aligning the lamp, measuring cell, and optical fiber optimally at the start of each experiment. The detector was gated with an EG&G 1302 pulse generator. The timing of the laser and optical multichannel analyzer (OMA) gate pulse was controlled by an EG&G OMA III model 1460 console with a 1303 pulse delay generator.

For measurements in the ns domain, the Xe lamp was pulsed to obtain sufficient measuring light, and a gate of 5 ns was used. In all other experiments, a gate of 10 μs was used, without pulsing the Xe lamp. In some experiments, the amount of Xe measuring light reaching the sample was minimized with a shutter that opened 100 ms before the laser pulse. To prevent complications (see Discussion), however, in all μs-to-s measurements analyzed below, the measuring light continuously illuminated the PYP sample. To obtain delays between the laser pulse and the gate pulse longer than 10 ms (the maximal delay of the OMA III console), a digital delay generator (EG&G model 9650) was used. This enabled us to sample the time range between 10 and 100 ms. To obtain difference spectra at delay times of hundreds of ms, the diode array signals were recorded at 100-ms time intervals 20 times after a single laser flash, allowing measuring times up to 2 s. In all other experiments each laser flash was associated with a single gate pulse, resulting in a measurement at a single time delay. The measurements were averaged over 10–20 flashes.

Due to the absence of a shutter in front of the Xe lamp, it was not possible to subtract a dark current from these two signals to correct for fluctuations in this background. To obtain a constant background the whole setup was shielded from external light. The fact that above 550 nm the signal showed a 0 baseline (see Results) indicated the adequacy of the measuring system. The room in which the apparatus was located was thermostated at $19 \pm 1°C$.

Routinely, the absorbance spectrum of the PYP sample just before and immediately after the measurements was recorded on an Aminco DW-2000 spectrophotometer (SLM Instruments, Urbana, Il) to check the photostability of the sample. The same apparatus was used to measure a high-resolution spectrum of the ground state of PYP.

Single-wavelength absorbance measurements

Time-resolved measurements at single wavelengths were performed on a different setup. A pulsed dye laser (PDL2, Quanta-Ray/Spectra Physics, dye: Coumarine 440) pumped by the third harmonic of an Nd:YAG laser (DCRA, Quanta-ray/Spectra Physics) operating at 0.25 Hz was used for excitation at 446 nm, and for excitation at 335 nm the light of the frequency-tripled Nd:YAG laser was used directly. Pulses of ~8 ns and an intensity of ~5–10 mJ were produced. To ensure a homogeneous distribution of excitation light a diffusor was placed on the entrance window of the sample

holder. The probe light was a 150-W tungsten halogen lamp. A ⅛ monochromator (Oriel, Stratford, CT) with a bandwidth of 18 nm was used to reduce the actinic effect of the probe light. No more than 1% of the PYP in the sample was excited into the photocycle by the continuous measuring light. The transmitted light was detected with a Hamamatsu (R456, Joko-cho, Japan) photomultiplier, with a response time of 3 μs. The detector was placed behind a ¼ monochromator (Photon Technology International, South Brunswick, NJ). The traces were recorded with a resolution of 3 nm, averaged 4–16 times, digitized by a Lecroy (Chestnut Ridge, NY) 99310 transient recorder, and stored on computer. Traces were measured at 23 different wavelengths in the 350–500-nm range. The sample was thermostated at 18.5°C. To check the photostability of the sample, absorption spectra were recorded on a Cary219 spectrophotometer (Varian, Mulgrave, Victoria, UK).

Data analysis

The basic model that describes the time evolution of spectra is the following (Notation convention: underlining indicates stochastic variables, uppercase represents matrices, lowercase represents scalars or vectors.).

$$\underline{\psi}_{t_i \lambda_j} = \sum_{l=1}^{n_{comp}} c_{lt_i} \epsilon_{l\lambda_j} + \underline{\xi}_{t_i \lambda_j} \tag{1}$$

$$\underline{\Psi} = CE^T + \underline{\Xi} \tag{2}$$

where the $m \times n$ matrix $\underline{\Psi}$ (with elements $\underline{\Psi}_{t_i \lambda_j}$) denotes the time resolved spectra, measured at m time instants t_i, and n wavelengths λ_j, c_{lt_i} denotes the concentration of component l at time t_i, $\epsilon_{l\lambda_j}$ denotes the contribution of component l at wavelength λ_j, and $\underline{\xi}_{t_i \lambda_j}$ denotes a gaussian-distributed stochastic disturbance with 0 mean. The c_{lt_i} and $\epsilon_{l\lambda_j}$ are gathered in the matrices C and E, of dimension $m \times n_{comp}$ and $n \times n_{comp}$, respectively, where n_{comp} is the number of components involved. Matrix $\underline{\Xi}$ represents the noise and is, like $\underline{\Psi}$, $m \times n$.

Regarding Eqs. 1 and 2 we note that the quantity that will be estimated is the product $c_l \epsilon_l^T$, which in itself is insufficient for the determination of the absolute values of c_l and ϵ_l. Thus when we have a kinetic model for c_l and no additional information we can only identify the parameters that determine its shape and not its absolute value. In our case we have additional information, namely, the ground-state spectrum, which can be used in a (subsequent) fit of the ϵ_l difference spectra. We will return to this identifiability problem later.

When the noise influences $\underline{\xi}_{t_i \lambda_j}$ are independent and normally distributed with unknown variance σ^2 across wavelength and time, the nonlinear least-squares estimator is the maximum likelihood estimator, and thus the best estimator. In difference absorption traces the noise variance usually varies as a function of wavelength, which necessitates a weighting based upon $\varsigma^2_{\lambda_j}$, which needs to be estimated as well. This procedure is called "iteratively reweighted least squares" (Weisberg, 1985).

Estimation of the number of components

In general, $\text{rank}(C) = \text{rank}(E) = n_{comp}$ and with perfect, noise-free data ($\Xi = 0$) we have $\text{rank}(\underline{\Psi}) = \text{rank}(CE^T) = n_{comp}$. Thus with experimental data of which we do not know the number of components it is necessary to estimate the rank of $\underline{\Psi}$. We estimate this rank using the singular value decomposition (SVD, Henry and Hofrichter, 1992; Malinowski 1991) of $\underline{\Psi}$

$$\underline{\Psi} = USW^T \tag{3}$$

where U and W are orthogonal matrices, respectively $m \times m$ and $n \times n$, whose columns contain the left and right singular vectors. S is an $m \times n$ matrix which is 0 except for its diagonal, which contains the singular values. With n_{comp} components and noise-free data we have exactly n_{comp} significant singular values: $s_1 \geq s_2 \geq \cdots \geq s_{ncomp} > s_{ncomp} + 1 = \cdots = 0$. When the SVD of $\underline{\Psi}$ results in n_{comp} singular values and singular vector pairs significantly different from noise we conclude that the system contains n_{comp} components. We routinely checked the absence of structure in the $n_{comp} + 1$-th left and right singular vectors by visual inspection.

To obtain insight in the $m \times n$ residual matrix $\underline{Z}$ resulting from a fit with a particular model, we calculated its SVD:

$$\underline{Z} = \underline{\Psi} - CE^{T} = \underline{U}_z \underline{S}_z \underline{W}_z^{T} \qquad (4)$$

The sum of squares of the residuals trace $(\underline{Z}^{T}\underline{Z})$ is equal to the sum of squares of the singular values, which we designate here Λ_z:

$$\Lambda_z = \sum_{i=1}^{\min(m,n)} s_{z,i}^2 \qquad (5)$$

Let us assume in the following that $n_{comp} = 2$. With a two-component model we could, in the ideal case, represent the data with the sum of the outer product of the first two singular vector pairs scaled with their singular values: $u_1(t)s_1w_1^{T}(\lambda) + u_2(t)s_2w_2^{T}(\lambda)$. Then the singular values of the residual matrix should be equal to $s_3,s_4, \cdots$ of the original data set. To judge the quality of the fit we compare $\Lambda_{\Psi,>2}$, which is defined as:

$$\Lambda_{\Psi,>2} = \sum_{j=3}^{\min(m,n)} s_j^2 \qquad (6)$$

with Λ_z. When the two are approximately equal we conclude that the fit is satisfactory.

Estimation of spectral and kinetic parameters

We now distinguish three different kinds of parametrizations (Van Stokkum et al., 1994), all of which we will apply to the PYP photocycle:

i) *A kinetic model.* The concentrations are described by a kinetic model, which depends on the nonlinear parameters θ, whereas the spectral parameters of the $n \times n_{comp}$ matrix E are simply linear parameters

$$\underline{\Psi} = C(\theta)E^{T} + \underline{\Xi} \qquad (7)$$

ii) *A spectral model.* The spectra are described by a parametric model, which depends on the nonlinear parameters θ, whereas the concentration parameters of the $m \times n_{comp}$ matrix C are simply linear parameters

$$\underline{\Psi}^{T} = E(\theta)C^{T} + \underline{\Xi}^{T} \qquad (8)$$

iii) *A spectrotemporal model.* Both the concentrations and the spectra are described by a model that depends on the nonlinear parameters θ. Assuming first-order kinetics, a matrix of linear parameters A describes the concentrations of the components in terms of a superposition of exponential decays, which are gathered in the matrix $C(\theta)$.

$$\underline{\Psi} = C(\theta)AE^{T}(\theta) + \underline{\Xi} \qquad (9)$$

The linear parameters (E in Eq. 7, C in Eq. 8, A in Eq. 9) can be eliminated in the nonlinear least-squares fit (Golub and LeVeque, 1979; Kaufman, 1975; Nagle, 1991; Van Stokkum et al., 1993). Furthermore, the estimated matrices E from Eq. 7 and C from Eq. 8 can in turn be fitted with, respectively, a spectral and a kinetic model. We have performed these types of analysis on the multichannel data of the PYP photocycle, as described below.

Compartmental models

For the kinetic model we take a linear compartmental model (Anderson, 1983; Godfrey, 1983) with n_{comp} compartments in which the differential equation for the concentrations is

$$\frac{d}{dt}c(t) = Kc(t) + j(t) \qquad (10)$$

where c and j are $n_{comp} \times 1$ vectors: $c = [c_1 \cdots c_{n_{comp}}]^{T}, j(t) = (t)[1 \cdots x_{n_{comp}}]^{T}$. $i(t)$ is the result of a convolution of the exciting laser pulse and the detector response, x_1 represents a possible extra input to compartment 1.

The solution to Eq. 10 is given by $c(t) = e^{Kt} \oplus j(t)$ where $\oplus$ indicates convolution. For a diagonal K matrix ($K = \text{diag}(\kappa_1, \cdots, \kappa_{n_{comp}})$, where $\kappa = -k$ is an eigenvalue) the concentration matrix C consists of elements $[C_1]_{pq} = c_q^1(t_p, k_q)$. The solution of the general compartmental model is a

linear combination of the c_1^1 and thus a transformation of C_1 (derived from the eigenvalues of the transfer matrix K) for which we can write $C_{II} = C_1A_{II}$.

A complication with the simultaneous analysis of multiple experiments are longterm fluctuations in, e.g., the laser energy, which necessitate the estimation of a scaling parameter for each extra experiment.

Spectral model

The shape of an absorption spectrum is often well described by a gaussian in the energy domain: $f(\bar{\nu})/\bar{\nu} = \epsilon_{max}\exp(-\ln 2[2(\bar{\nu} - \bar{\nu}_{max})/\Delta\bar{\nu}]^2)$ where $\bar{\nu} = \lambda^{-1}$ denotes the wave number and $f(\bar{\nu})$ is the converted absorption spectrum: $f(\bar{\nu}) = \lambda^2\epsilon(\lambda)$ (Lakowicz, 1983). Even better fits are achieved when an extra skewness parameter is introduced (Fraser and Suzuki, 1969; Sevilla et al., 1989). Thus we arrive at the model function

$$\epsilon(\bar{\nu}) = \bar{\nu}^3\epsilon_{max}\exp(-\ln 2[\ln(1 + 2b(\bar{\nu} - \bar{\nu}_{max})/\Delta\bar{\nu})/b]^2) \qquad (11)$$

Note that with skewness parameter $b = 0$ the exponent in Eq. 11 reduces to a gaussian. In modeling an absorption difference spectrum the ground-state spectrum ϵ_0 is subtracted from a linear combination of $\epsilon(\bar{\nu})$ as in Eq. 11:

$$\epsilon(\bar{\nu}; (\bar{\nu}_{max}, \Delta\bar{\nu}, b)_1, \cdots, (\bar{\nu}_{max}, \Delta\bar{\nu}, b)_M, a_1, \cdots, a_M)$$

$$= \sum_{m=1}^{M} a_m \bar{\nu}^3 \exp\left(-\ln 2 \left[\frac{\ln(1 + 2b(\bar{\nu} - \bar{\nu}_{max,m})/\Delta\bar{\nu}_m)}{b_m}\right]^2\right) - \epsilon_0 \qquad (12)$$

which depends upon $4M$ nonlinear parameters. Each component can have a different M, e.g., with $M_1 = 1$ and $M_2 = 2$ we have 12 nonlinear parameters, which is much larger than the number of nonlinear parameters with a kinetic model.

Equivalence of spectral or temporal models

Because of the linearity of the model function the decomposition of Ψ into the product of two matrices is problematic. Let A be an invertible matrix then:

$$CE^{T} = CAA^{-1}E^{T} = (CA)(EA^{-T})^{T} \qquad (13)$$

Because we are dealing with a model function CE^{T} the linear combinations of spectral or temporal models will produce exactly the same residuals. For instance, a two-component kinetic model C_1 results in decay associated spectra (Knutson et al., 1983) E_1. An alternative model II where the second component is formed from the first component $C_{II} = C_1A_{II}$ (Van Stokkum et al., 1993) leads to the same estimated kinetic parameters, but a different spectrum of the first component $E_{II} = E_1A_{II}^{-T}$. A priori knowledge about E (e.g., nonnegativity of the $\epsilon_1(\lambda)$) offers us the possibility to choose between alternative models. With a spectral model an analogous problem exists; in this case the estimated concentrations need to be nonnegative. Our approach in dealing with the fundamental problems associated with the identification of the kinetic and spectral characteristics of the individual components involved in the PYP photocycle was the application of different types of models with fundamentally different assumptions (either on the kinetic behavior of the intermediates or on their spectral characteristics or both). The consistency of the conclusions drawn from the different approaches can be examined by a comparison of results obtained with different models.

Analysis of the first left singular vector

As described above, the kinetic model consists of a superposition of exponential decays. To investigate automatically the optimal number of discrete decays we applied the DISCRETE program (Provencher and Vogel, 1980) to the first left singular vector of the trace data, given that this vector represents the main temporal changes and possesses a high signal-to-noise ratio. Note that the number of decays can be larger than the number of spectrally different components. In addition we fitted this vector with the

CONTIN program to obtain a continuous distribution of rates of exponential decay (Provencher, 1982).

RESULTS

Time-resolved multichannel absorbance measurements

We have measured laser pulse-induced absorbance changes in PYP on an ns-to-s time scale. To achieve this, the experiments were divided into seven time domains covering the 1–25-ns and 10 μs-2-s ranges. We first describe the data keeping in mind the available knowledge (Meyer et al., 1987, 1989). Excitation of PYP with an 8-ns (full width at half maximum) laser pulse at 446 nm results in the formation of a red-shifted intermediate (Fig. 1 a). Experiments performed at the maximum time resolution of the apparatus used (a 5-ns gate with a 1-ns increment delay) showed that this bathointermediate is formed in parallel with the risetime of the laser pulse, indicating that this transition was not time resolved and must be faster than 1 ns. Additionally, a fluorescence emission signal, causing an apparent bleaching at 500 nm, was observed. Singular value decomposition of the ns data, which were analyzed separately from the μs-to-s data, in-

dicated that three components were present in this initial process (Fig. 1 b). These could be ascribed to the rise and decay of the laserflash artifact at 446 nm, fluorescence from the excited state with a maximum at about 493 nm, and the formation of a red-shifted intermediate with concurrent bleaching of the groundstate. The time constants of these processes were beyond the time resolution of our apparatus.

The μs-to-s dataset contains two components, as was concluded from the singular value decomposition (Figs. 1 d and 2 d). First, the red-shifted intermediate decays in the sub-ms time range to a blue-shifted intermediate, with an isosbestic point at ~395 nm (Fig. 1 c). This isosbestic point is in agreement with the assumption that the conversion from the red to the blue intermediate takes place in a single transition. The last step in the photocycle is the recovery of the ground state of the protein from the blue intermediate, with a sub-s rate (Fig. 1 e). This process is isosbestic at ~385 nm. This suggests that the single component involved in this recovery (Fig. 1 f) directly gives the absorption difference spectrum of the blue intermediate. However, an equilibrium in which some red-shifted intermediate is still present cannot be excluded. All μs-to-s multichannel absorbance measurements are concatenated and depicted in Fig. 2 a.

FIGURE 1 Multichannel measurements of the absorbance changes during the PYP photocycle. Different line types indicate successive times in the order solid, dotted, dashed, dot-dashed, and chain-dashed. In (a) measurements in the ns range are shown starting at 12 ns and with 3 ns intervals (N.B., the tail of the laser flash is visible in the first three spectra). Measurements in the range from 50 μs to 0.85 ms with 200-μs intervals are presented in (c), showing the transition from a red-shifted to a blue-shifted intermediate. Measurements of the last stage of the photocycle are shown in (e), from 50 ms to 0.85 s with 200-ms intervals. The singular values of these three data sets are shown (on a logarithmic scale) in (b), (d) and (f), respectively.
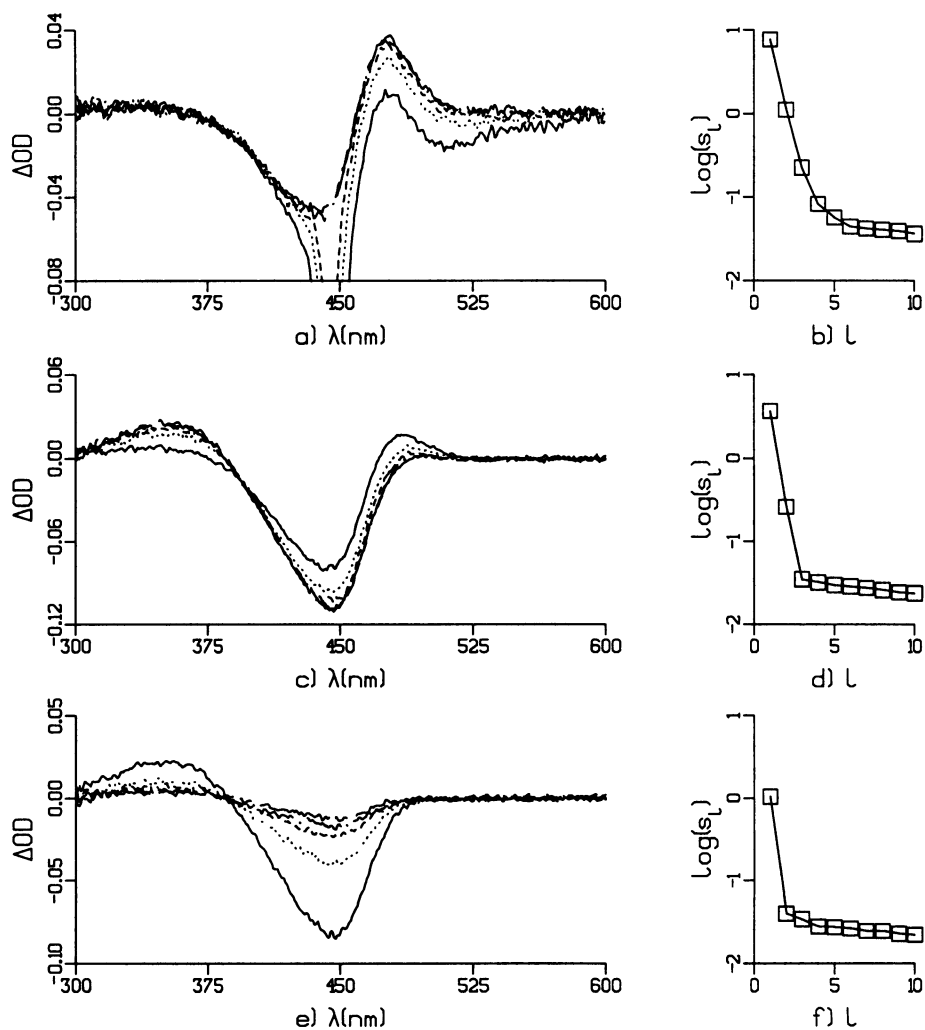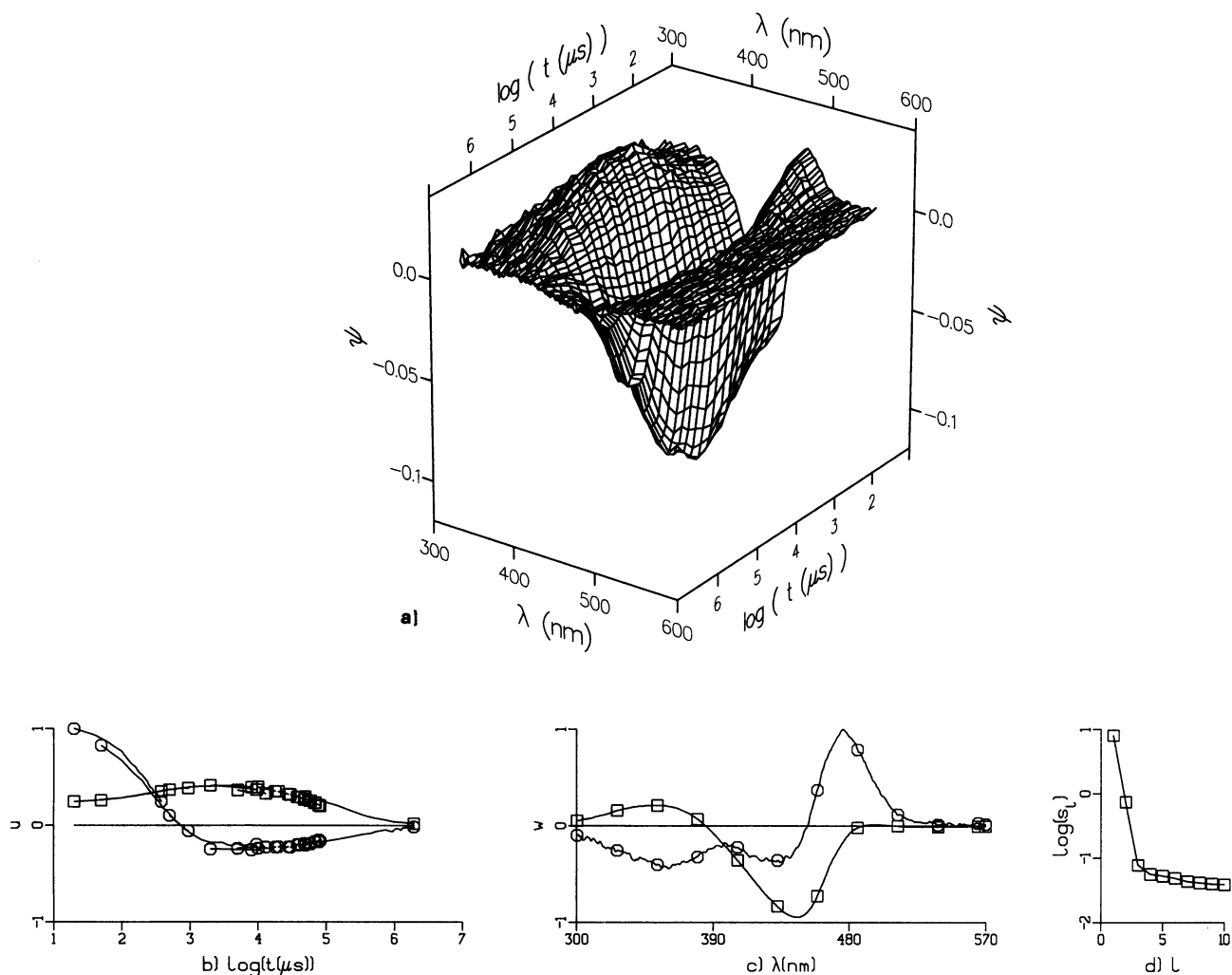
FIGURE 2   Absorbance changes Ψ during the PYP photocycle measured with a multichannel analyser set-up. In (a) a subset of the complete μs-to-s dataset is shown in a three-dimensional plot. The singular value decomposition indicates the presence of two intermediates. First ($\square$) and second ($\bigcirc$) left (u) and right (w) singular vectors are shown in, respectively, (b) and (c). Lines connecting symbols in (b) indicate separate experiments. (d) Singular values s_1 (on a logarithmic scale).

Global analysis of the multichannel absorbance measurements

We have first globally analyzed the OMA data using the model of Meyer et al. (1987, 1989, 1991), in which a red intermediate ($\square$ in Fig. 3, a and b) is formed, which decays exponentially to the blue intermediate ($\bigcirc$ in Fig. 3 a and b), which in turn decays exponentially to the ground state. The results shown in Fig. 3 are unsatisfactory as judged from the residuals. To obtain insight in these residuals, we analyzed the matrix of residuals with the help of the SVD (Eq. 4). With this two-component model, in the ideal case, the singular values of the residual matrix should be equal to $s_3, s_4, \cdots$ of the original data set (see data analysis section). Comparing Fig. 3 e with Fig. 2 d we see that this is clearly not the case: s_1 of the residuals is between s_2 and s_3 of the original data set. The first right singular vector of the residuals w_{res} (Fig. 3 d) resembles its counterpart of the full data set w_1 (squares in Fig. 2 c), and is clearly different from noise. The first left

singular vector of the residuals (Fig. 3 c) is also highly structured, in particular at times larger than 100 ms. It was already clear from visual inspection of the data that there was still some signal present at times longer than 1 s (Fig. 1 e and Fig. 2 a). Furthermore, Λ_Z (see the Data Analysis section) was found to be $13.7 * 10^{-2}$, much larger than the $\Lambda_{\Psi,>2}$ of $6.5 * 10^{-2}$ indicating the inadequacy of the model.

We now turn to a spectral model of the difference absorbance spectra. Fig. 4 a shows the fit of the ground state spectrum ϵ_0 with a superposition of two skewed gaussians (dashed lines, parameters in Table 1) of Eq. 11. The accompanying residuals in Fig. 4 b are small but still somewhat structured. This may well be caused by vibrational fine structure of the supposed polyene chromophore in PYP. This is reminiscent of the vibrational fine structure observed at 77 K (Hoff et al., 1992). We fitted the estimated difference spectra of Fig. 3 b using the spectral model of Eq. 12. The red intermediate was well fitted using a superposition of two
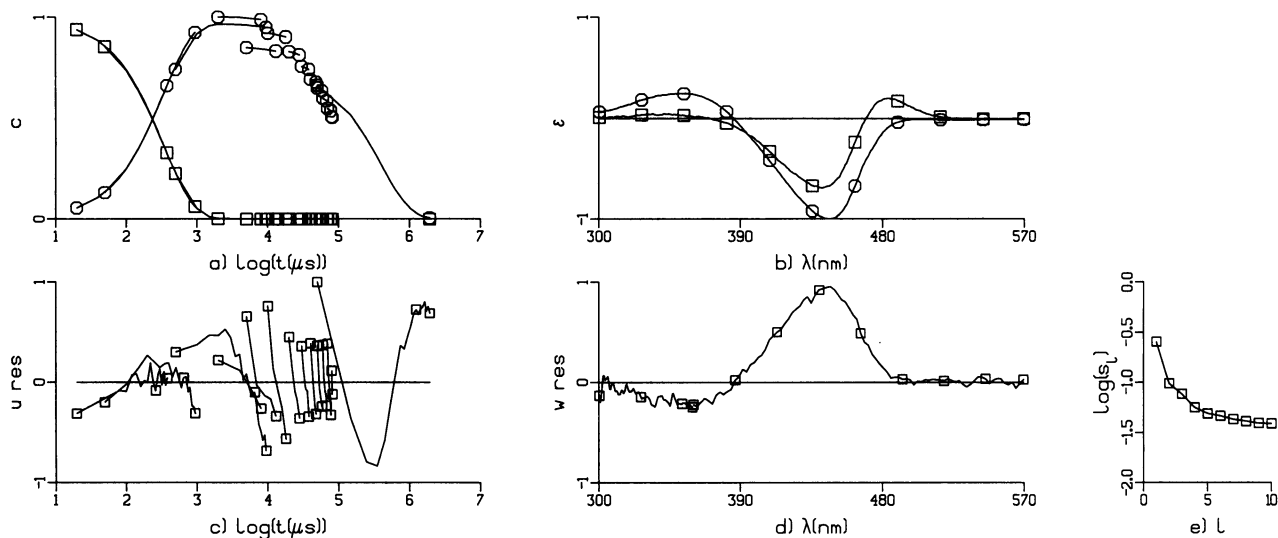
FIGURE 3 Global analysis of µs-to-s OMA dataset of the absorbance changes in the PYP photocycle with a two-step kinetic model. In (a) the concentration profiles c of the intermediates (□, red; ○, circles) are shown, and (b) shows the accompanying difference spectra ε. The results of the SVD of the residuals in the time and wavelength domain are shown with first left (u_{res}, c) and right (w_{res}, d) singular vectors, as well as the singular values s_l (on a logarithmic scale) (e). Lines connecting symbols in (a) and (c) indicate separate experiments.
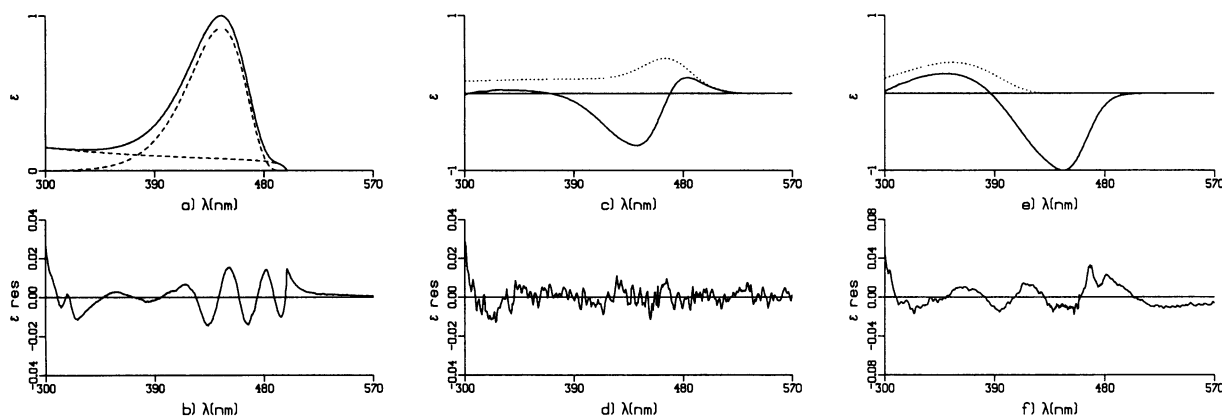

FIGURE 4 Fit results of the absorption spectra of the three states of PYP. Vertical scale relative to maximum of ϵ_0. (a) fit of ground state spectrum ϵ_0 with two skewed gaussians (dashed lines). (b, d, f) accompanying residuals. (c, e) fit of difference spectrum (solid) of respectively, red and blue intermediate of Fig. 3 b resulting in dotted spectrum.

TABLE 1   Parameters of spectral fit of ground state spectrum ϵ_0

λ_{max} (nm)	$\bar{\nu}_{max}$ (10^3 cm^{-1})	$\Delta\bar{\nu}$ (10^3 cm^{-1})	b	a_2/a_1
445	22.29	2.53	0.50	
	21.44	7.0	2.5	0.087

skewed gaussians (Fig. 4, c and d). The blue intermediate was fitted with a single band (Fig. 4 c). However, the residuals ~480 nm (Fig. 4 f) are problematic, indicating that there may be some extra absorbance present in the red during the recovery phase.

A natural way to analyze the time-gated spectra is the spectral model (Eqs. 8 and 12). The results shown in Fig. 5 are again unsatisfactory, partly for the same reasons. Fitting the concentration parameters from Eq. 8 with a kinetic

model, the blue intermediate (circles in Fig. 5, a and b) shows a biexponential recovery to the ground state (not shown). The first singular value of the residuals (Fig. 5 e) is smaller than with the kinetic model (Fig. 3 e) but still too large (compare with s_3 in Fig. 2 d). In agreement with this, the Λ_Z equaled $9.5 * 10^{-2}$, smaller than with the kinetic model but still larger than the $\Lambda_{\Psi,>2}$ of $6.5 * 10^{-2}$. Furthermore, the shape of the first left singular vector of the residuals resembles the shape of the concentration of the blue intermediate (circles in Fig. 5 a), and the first right singular vector is reminiscent of the problems with the fit of the difference spectrum of the blue intermediate in Fig. 4 f. In Fig. 5 a we have also drawn the sum of the estimated concentrations of the two components (indicated by triangles). This sum should be constant up to at least 1 ms, but appears to be rising. This clearly violates the conservation of photocycle states.
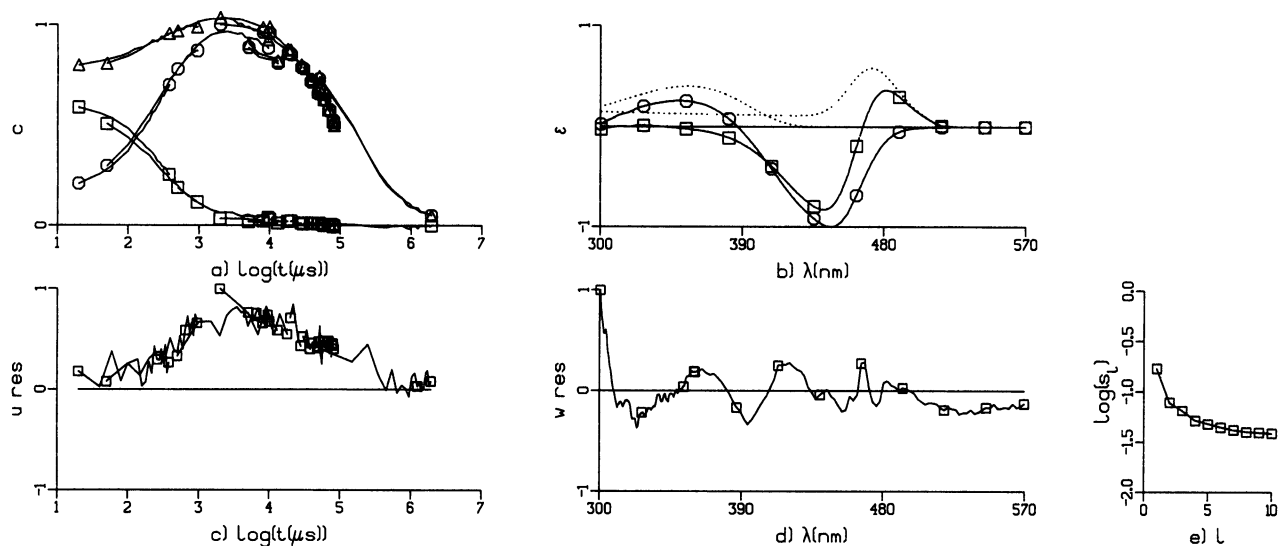
FIGURE 5   Global analysis of μs to s OMA dataset of the absorbance changes in the PYP photocycle with a spectral model. Lay out as in Fig. 3. (*a*) $\triangle$, sum of concentrations of red ($\square$) and blue ($\bigcirc$) intermediates. Solid lines in (*b*) represent fitted difference spectrum, dotted lines indicate spectra of intermediates.

We combined the two models for a selected time range of 20–380 μs where we performed a spectrotemporal fit, with A in Eq. 9 equal to a scalar constant. The residuals here are much more satisfactory (Fig. 6, *c–e*); in this case $\Lambda_{\Psi,>2}$ was $6.5 * 10^{-3}$ and Λ_Z was $8.9 * 10^{-3}$. The parameters estimated from these fits are compiled in Table 2. Note that the estimates of the amplitude (relative with respect to ϵ_0) of the spectrum of the red intermediate, which overlaps with ϵ_0, vary from 0.45 to 0.58, whereas λ_{max} varies from 460 to 472 nm. The spectrum of the blue intermediate appears to be better determined (amplitude 0.40–0.41, λ_{max} 355–357 nm). The estimated $k_{R \to B}$ varies from 2.4 to 2.9 $\times$ 10^3 s^{-1}, whereas the recovery is biexponential.

Four more comparable OMA experiments (not shown) were performed and analyzed, which strengthened the above conclusions drawn from Table 2.

Single wavelength absorbance measurements

To complement the analysis of the photocycle in PYP from *E. halophila*, we have also performed time-resolved single wavelength absorption measurements. Whereas the multichannel measurements yield data with a high spectral resolution, these single wavelength traces have a higher time resolution. In addition, the amount of measuring light reaching the sample is much smaller. This may be advantageous, given that the measuring light itself could have a complicating effect on the photocycle because of the photosensitivity of the intermediates (Hoff et al., 1992; Miller et al., 1993).

The dataset obtained by these measurements (Fig. 7 *a*) showed the same characteristics as observed with the OMA measurements: the immediate formation of a red-shifted
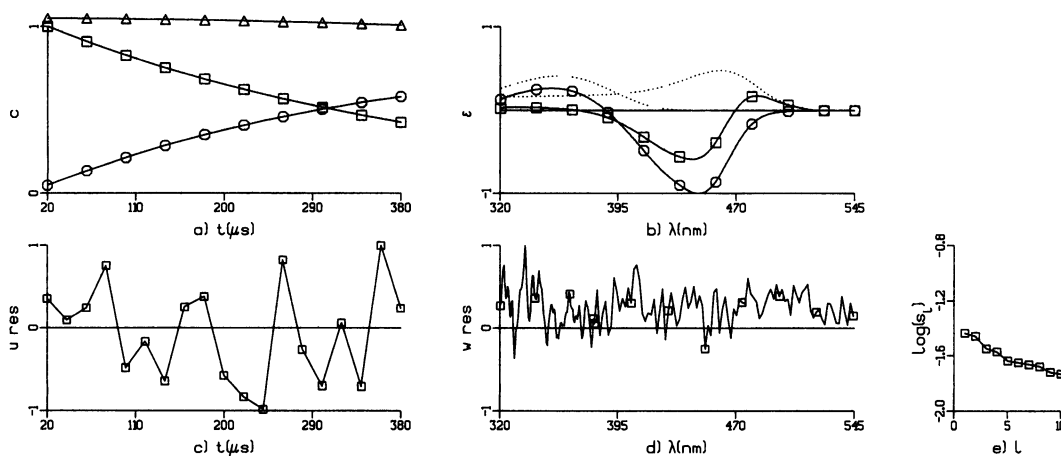

FIGURE 6   Global analysis of 20–380 μs OMA dataset of the absorbance changes in the PYP photocycle with a spectrotemporal model. Layout as in Fig. 5.

TABLE 2 Parameter fit results with the OMA dataset of Fig. 3 (further explanation in text)

Model	$k_{R \rightarrow B}$ (10^3 s^{-1})	$k_{B \rightarrow G}$ (s^{-1})	ϵ_{rel}	λ_{max} (nm)	$\bar{\nu}_{max}$ (10^3 cm^{-1})	$\Delta\bar{\nu}$ (10^3 cm^{-1})	b	a_2/a_1
Kinetic	2.9	2.5	0.40	355	27.29	6.02	0.55	
			0.45	465	21.31	1.95	0.22	
					22.1	7.3	1.09	0.47
Spectral	2.5	5.5 (76%)	0.40	355	27.28	6.03	0.54	
		0.75 (24%)	0.58	472	21.10	1.61	0.00	
					21.17	6.4	1.8	0.19
Spectrotemporal	2.4	*	0.41	357	27.26	5.70	0.43	
			0.48	460	21.54	2.24	0.38	
					21.67	6.34	1.22	0.51

* Because the spectrotemporal fit was done for a selected time range of 20–380 μs the recovery rate could not be estimated.
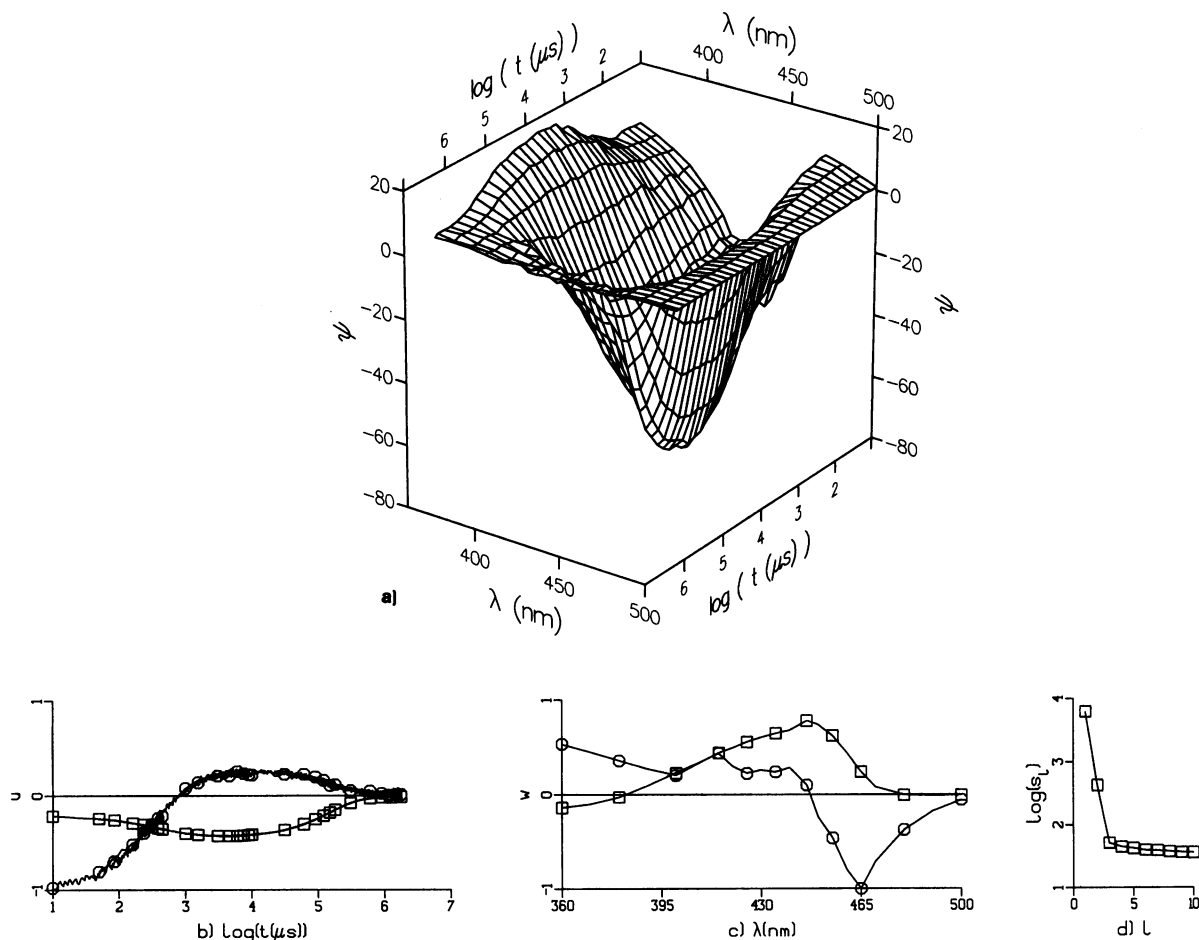

FIGURE 7   Absorbance changes Ψ during the PYP photocycle as measured with single-wavelength setup. A representative subset of the data was chosen for clarity. Layout as in Fig. 2.

intermediate that decays to a blue-shifted intermediate at a sub-ms timescale, followed by the recovery of the ground state at a sub-s time scale. Again the SVD indicated the presence of two components significantly different from noise (Fig. 7, b–d). The signs of the singular vectors are reversed as compared with Fig. 2, b and c, which is explained by the sign indeterminacy of the SVD.

In another experiment we excited at 355 nm. When relatively low pulse intensities and a diffusor were used, the sample was not photodestructed and normal photocycle signals were measured (not shown). At higher pulse energies

and without diffusor, the sample did show significant photodestruction.

Global analysis of the single wavelength measurements

The single-wavelength measurements were analyzed in a manner that is closely parallel to that used for the OMA measurements. The two-compartment kinetic model yielded fits (Fig. 8, a and b) with parameters similar to those found for the OMA data (see Table 3, upper part). As described in
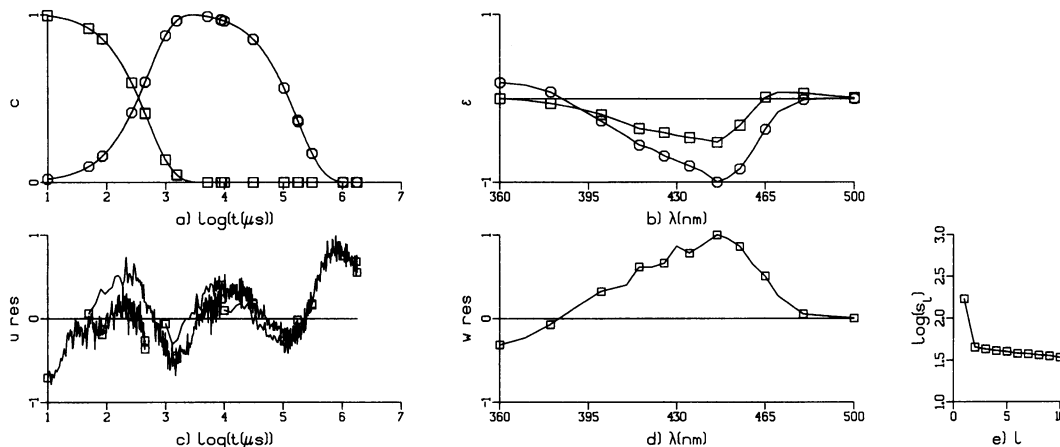
FIGURE 8   Global analysis of μs to s traces dataset of the absorbance changes in the PYP photocycle with a two-step kinetic model. Layout as in Fig. 3. In (c), (d), and (e), the SVD of the unweighted residuals is represented.

TABLE 3   Parameter fit results with the single wavelength dataset of Fig. 8 (further explanation in text)

Model	$k_{R \to B}$ (10^3 s^{-1})	$k_{B \to G}$ (s^{-1})	ϵ_{rel}	λ_{max} (nm)	$\bar{\nu}_{max}$ (10^3 cm^{-1})	$\Delta\bar{\nu}$ (10^3 cm^{-1})	b	a_2/a_1
Kinetic	2.02	5.73	0.38	370	27.1	4	0	
			0.5	465	21.4	1.1	0.6	
					21	4	2	0.4
kinetic*	3.93 (60%)	6.68 (93%)						
	0.85 (40%)	0.50 (7%)						

* Results from a global analysis with two biexponential decays.

the Data Analysis section we used a weighting based upon a wavelength-dependent variance. For the SVD analysis we used the unweighted residuals.

The residuals of this fit are clearly structured (Fig. 8, c–e), indicating that this model does not completely describe the data set. $\Lambda_{\Psi,>2}$ was 2.0×10^4, much smaller than the Λ_Z of 5.0×10^4. The spectral fit of the difference absorption spectra was not very satisfactory (Fig. 9). In particular the recovery spectrum showed large residuals ~460 nm (Fig. 9 d), indicating again that some red intermediate may be present.

As described in the theoretical methods, the first left singular vector ($\Box$ in Fig. 7 b) was fitted with an automatically

determined discrete sum of decays, and with a continuous distribution of decays. The residuals with five decays (Fig. 10 b) showed some small trends that were removed when fitting with a 31-point distribution. The difference between the two types of residuals is shown in Fig. 10 d. The five discrete decays found coincided with five extrema in the distribution (compare Fig. 10, c and e). Thus inspired, we performed a global analysis with five exponential decays. The residuals of this fit were satisfactory (Fig. 11, c–e). In particular, the singular values of the residuals (Fig. 11 e) resemble the s_3, s_4, $\cdots$ of the original data set (Fig. 7 d) and now Λ_Z was 2.0×10^4, which is identical to $\Lambda_{\Psi,>2}$. The large

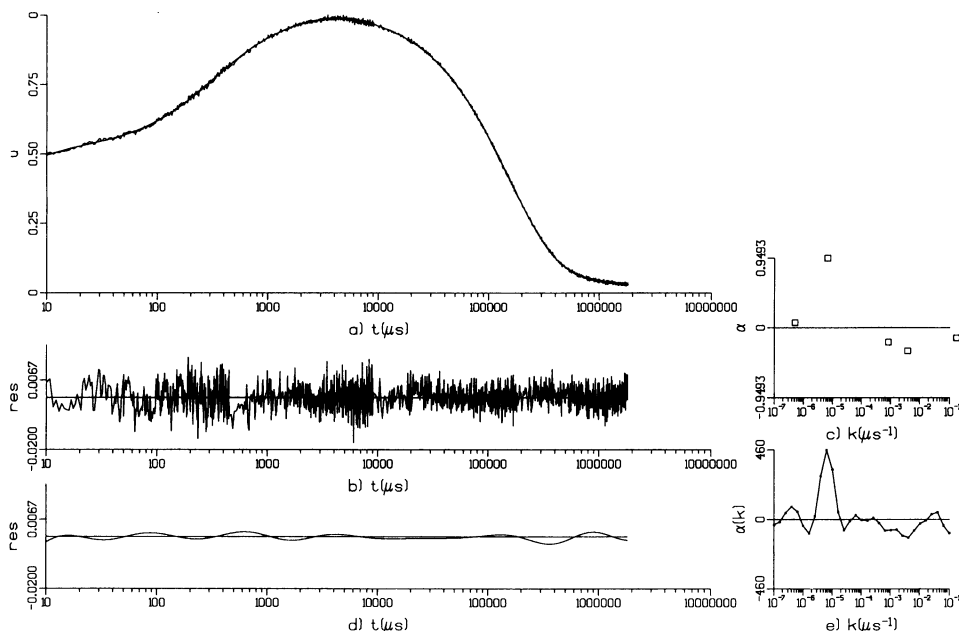FIGURE 9   Spectral fit of difference spectra of Fig. 8 b. Layout as in Fig. 4, c–f.
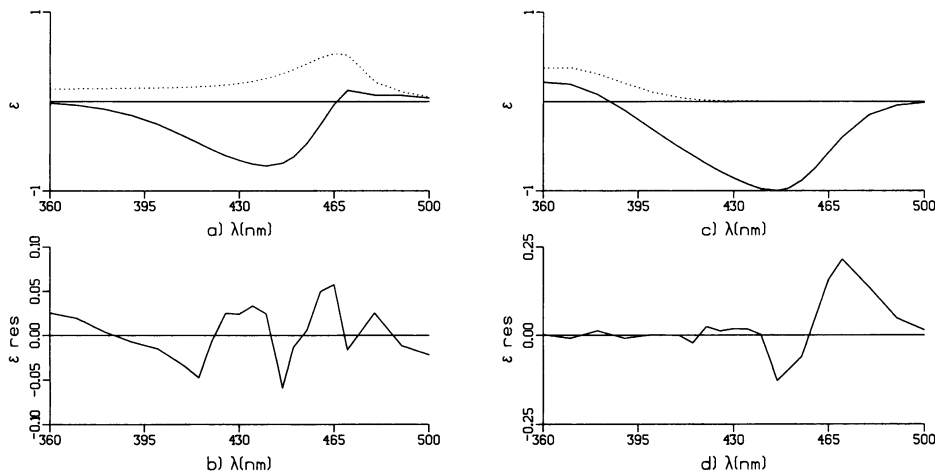
FIGURE 10   Fit of first left singular vector u_1 (squares in Fig. 7 b) with discrete sum of decays (b, c), and with a continuous distribution of decays (d, e). The residuals of the DISCRETE fit are shown in (b) and the difference between the residuals from a continuous and discrete fit are depicted in (d). Amplitudes α and rates k of the five exponential fit are shown in (c), and the distribution $\alpha(k)$ as a function of rate k is depicted in (e).
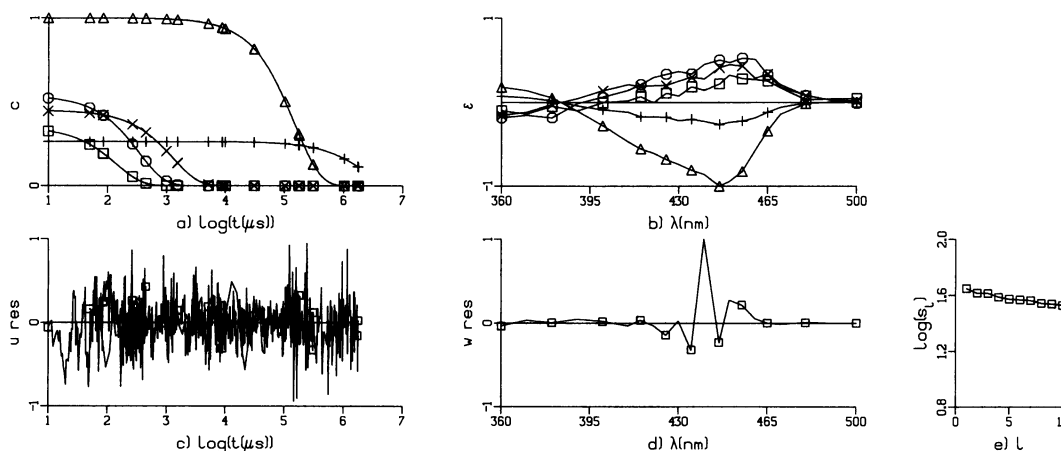

FIGURE 11   Global analysis of trace data using five independent decays. Layout as in Fig. 8. Decay-associated spectra in (b) are indicated by symbols that correspond to the symbols of the decays in (a). The curves are scaled according to their contribution to the data (Van Stokkum et al., 1993).

variance of the unweighted residuals ~446 nm (Fig. 11 d) can be explained by the reduced signal-to-noise ratio due to the ground-state absorbance. Omitting the smallest and fastest decay ($\Box$ in Fig. 11, a and b) gave only a tiny increase in the residuals, which still appeared satisfactory (not shown). Interestingly, the shapes of the four remaining decay-associated spectra in Fig. 11 b showed a great resemblance pair by pair ($\bigcirc$, $\times$, interconversion decays (R $\rightarrow$ B); $\triangle$, $+$, recovery decays (B $\rightarrow$ G)). However, when we fitted with a two-component model, both biexponential decays (lower part of Table 3), the residuals became less satisfactory (not shown) with a Λ_z of 2.1 $*$ 10^4, but of course still much better than with the two-step model of Fig. 8.

The experiment with 355-nm excitation mentioned above also indicated that two-plus-two decays are necessary to fit the data (not shown).

DISCUSSION

Only a small number of photoactive proteins are known and even fewer, the retinal proteins (Birge, 1990; Lanyi, 1992; Mathies et al., 1991; Stavenga et al., 1991) and phytochromes (Braslavsky, 1990) have been studied in molecular detail. After absorption of a photon by the chromophoric group these proteins undergo a series of dark reactions during which changes occur in a protein's absorbance spectrum,

caused by the chromophore and its interaction with the protein. When these dark reactions result in the reformation of the initial state of the protein, the overall process is called a photocycle. The absorbance changes associated with such a photocycle can occur because of reversible, photochemically induced changes in the structure of the chromophore, by changes in the conformation of the polypeptide chain, or by a combination of these two processes. Generally, this results in changes in the position of the absorbance maximum and/or in changes in the magnitude of the molar extinction coefficient. Therefore, these processes can be studied in detail by time-resolved difference absorbance spectroscopy.

To obtain a detailed understanding of a photocycle, it is necessary to elucidate the number of intermediate states that are involved in this process and to obtain spectral and kinetic information on these intermediates. For a number of reasons it is difficult to extract such a spectral and kinetic description of a photocycle from the raw data. First, the absorbance spectra of the different intermediates often show large overlap both spectrally and temporally, resulting in a situation in which at many wavelengths and time intervals more than one intermediate contributes to the absorbance signal measured. These contributions can only be resolved by incorporating additional independent spectral and/or kinetic knowledge, a model, into the data analysis procedure. Second, it may be difficult to test the assumptions that have to be made to perform such a data analysis.

The methods to analyze data sets containing flash-induced time-resolved difference absorbance spectra have been extensively applied to bR. This protein has also served as a model system for the further development of global analysis techniques (Hessling et al., 1993; Nagle, 1991; Zimányi and Lanyi, 1993). However, in spite of two decades of intense investigations, the exact photocycle scheme of bR is still somewhat controversial. Particularly difficult issues are the existence of parallel photocycles and the degree of reversibility of the different steps in the bR photocycle (Eisfeld et al., 1993; Lozier et al., 1992; Váró and Lanyi, 1991). As has been discussed in the Data Analysis section of Materials and Methods (around Eq. 13), different models can give rise to equally good fits even though such models may be spectrally and/or kinetically (in terms of microscopic rate constants) distinct.

We have collected and analyzed two independent data sets on the absorbance changes associated with the PYP photocycle, one with optimal spectral resolution and the other with optimal temporal resolution. We have analyzed these two data sets separately and have applied a number of different models to fit these data. This has allowed us to compare the results of these different procedures as a test for the consistency of the results obtained.

The first step in our analysis is the estimation of the number of independent components that are involved in the PYP photocycle. The SVD of both data sets presented above strongly indicated that only two spectrally and kinetically distinct intermediates are involved in the PYP photocycle in the μs-to-s domain (see Figs. 2 d and 7 d). The ns data set

(Fig. 1 a) indicated that the formation of the red-shifted intermediate is beyond the time resolution of our experimental setup. Given that the red-shifted intermediate is stable on an ns timescale, we focused on the processes occurring on the μs-to-s timescale.

By applying a spectral or spectrotemporal model on the multiple-wavelength data sets, we were able to estimate the absolute spectra of the two intermediates involved (Figs. 4, c and e; 5 b; 6 b, and 9, a and c). The different models and data sets resulted in a coherent set of estimated absorbance spectra for the two intermediates: in all cases a short-lived, red-shifted intermediate (λ_{max} = 460–472 nm and ϵ_{rel} = 0.45–0.58) and a long-lived, blue-shifted intermediate (λ_{max} = 355–357 nm and ϵ_{rel} = 0.40–0.41) were found. This is in full agreement with previous proposals (Meyer et al., 1987; 1989; 1991). However, the results obtained with the three different kinds of parameterizations of a single data set are not identical (Table 2). This underlines the paramount importance of starting with the most suitable model. Choosing a kinetic model fixes the difference spectra (Eq. 7), whereas choosing a spectral model fixes the concentration matrix (Eq. 8). There is no model-independent approach (Hessling et al., 1993; Zimányi and Lanyi, 1993) to analyzing such data. In particular with photocycles in which it is difficult or impossible to measure the pure spectra of the intermediates separately, it is always necessary to use knowledge, preferably in the form of a parameterized model, to decompose the data set satisfactorily.

The absorbance spectra of the intermediates that we have estimated underscore the close photochemical analogy between PYP and bR and the sensory rhodopsins. In terms of rate of formation (k), position of the absorbance maximum (λ_{max}), and molar extinction coefficient (ϵ_{rel}), the red-shifted PYP intermediate would correspond to the K intermediate of bR, whereas these three criteria associate the blue-shifted PYP intermediate with the M intermediate of the bR photocycle. Additionally, we have obtained some indications that, as in the bR photocycle, reversibility may play a role in the PYP photocycle: the residuals shown in Figs. 4 f and 9 d may indicate that during the transition of the blue-shifted intermediate to the ground state of PYP some red-shifted intermediate is still present.

An unexpected complication was encountered when a kinetic model with two sequential compartments was applied. The fits obtained with this model resulted in strongly structured residuals (Figs. 3, c and d; and 8, c and d). Closer examination of the data with the programs CONTIN and DISCRETE showed that at least four rather than two rate constants are present in the single-wavelength dataset. In the multichannel dataset only three rate constants were resolved, but it should be realized that data with a very good time resolution and signal-to-noise ratio are needed to resolve the four rate constants. When trace experiments were analyzed in which fewer traces were averaged, the structure in the residuals was almost completely obscured by the noise. However, analysis of the first left singular vector of such data again indicated four rate constants.

These results indicate that in the case of the PYP photocycle it is appropriate to use exponential models instead of a distributed kinetics approach, as can be concluded by the results with CONTIN that indicate the presence of four separated peaks in a fit with a continuous distribution of rate constants (see Fig. 10). The occurrence of four separate lifetimes was even more apparent from fits on partial datasets with a narrower time range (not shown). However, it cannot be excluded that especially for the formation of the blue-shifted intermediate a distribution of decay rates is involved (Ansari et al., 1985). A fit with four monoexponential decays indicated that the resulting decay-associated spectra separated in two pairs of very similar shape, supporting the SVD. This result indicates that, although the spectral aspect of the dataset appears to be well understood, the kinetics are more complicated than expected. Unfortunately, the underlying chromophore (photo)chemistry of PYP has not yet been resolved (Van Beeumen et al., 1993). The PYP photocycle is schematically depicted in Fig. 12.
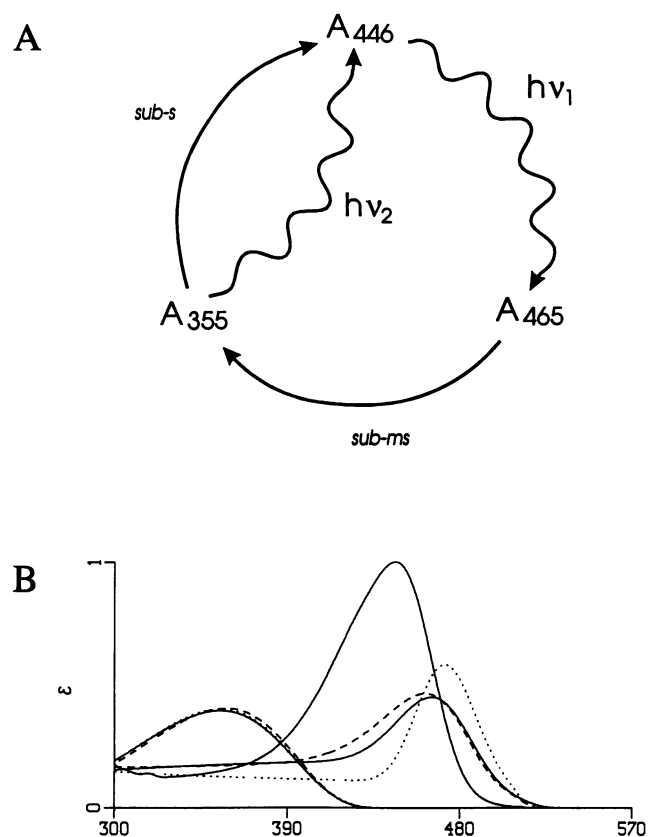

FIGURE 12 Schematic representation of the PYP photocycle. In (A) the thermal and light-induced reactions between the different intermediates occurring in the room temperature photocycle of PYP are depicted. In (B) the estimated absorbance spectra of the two photocycle intermediates in the PYP photocycle resulting from three different models are shown together with the measured ground state absorbance spectrum (scaled). Different line types indicate different models (see text for explanation): kinetic (solid), spectral (dotted), and spectrotemporal (dashed). Note that the spectrotemporal fit was performed on a restricted time domain (20–380 μs).

We have found no straightforward physical interpretation of these data. The possible explanations that we have considered and subsequently rejected are the following. An experimental error seems unlikely given that the conclusions from the analysis are essentially identical for the two different setups used and for two proteins batches that were isolated independently. Partial degradation of the protein can be excluded because independent, fresh PYP isolates were used for the experiments, and electrospray mass analysis of the protein samples indicated the absence of significant proteolysis upon completion of the measurements. In addition, the samples were spectrally checked for photostability regularly. The occurrence of branching photoreactions from both the red- and the blue-shifted intermediates have been reported (Hoff et al., 1992; Miller et al., 1993). However, because the measuring light that could initiate these processes was constantly illuminating the sample, no additional lifetimes can arise through these processes. This is a direct consequence of the fact that the number of time constants in the measured data is always smaller than, or equal to, the number of compartments in the reaction scheme (Anderson, 1983; Godfrey, 1983; Nagle, 1991). In the worst case, different numerical values for the lifetimes involved would be the result of these light-induced branching reactions. (This is not the case for the data presented above, because variation of the measuring light intensity (not shown) did not significantly affect the numerical values of the measured rate constants.) Therefore, the four decay rates found imply that in terms of compartmental models four compartments are needed to describe the PYP photocycle. In such a case solving for a complete K matrix (Eq. 10) is difficult (Nagle, 1991). For example, with phytochrome it has been difficult to distinguish between different kinetic models that can explain multiexponential behavior (Scurlock et al., 1993).

This situation is unaffected by the ways in which the different compartments are connected through the microscopic rate constants of the system (by light-induced or dark reactions). This argument excludes the occurrence of reversibility in the photocycle as an explanation for the occurrence of the two additional rate constants. Another possibility could be that rotational diffusion processes of the intact protein contributed to the difference spectra, as we have not measured at the magic angle. However, these processes are expected to be much faster than the time constants observed given that PYP is a small, water-soluble protein. The results with fits using a distribution of lifetimes indicated that in the case of PYP it is not necessary to use distributed kinetics models: four separated time constants were observed. The last possibility we have considered is that of conformational heterogeneity of PYP, leading to a number of different, parallel photocycles. However, this type of explanation is not straightforward because of the large difference in the relative amplitudes of the two fast and the two slow processes (60 and 40% and 93 and 7%, respectively) observed in this study and of 85 and 15% observed previously for fast phase heterogeneity (Meyer et al., 1987) and no heterogeneity at all with

one protein preparation (Meyer et al., 1989). There also appears to be a variation in rate constants from one preparation to another, which may be caused by slight variations in the composition of the solvent used in the different studies or to an as yet unexplained source of heterogeneity. Therefore, the precise physical interpretation of the PYP photocycle in terms of an exact photochemical reaction scheme, which may involve protein conformational heterogeneity and the spectroscopically silent population of compartments not depicted in Fig. 12 by the measuring light, will have to await further biophysical experimentation.

REFERENCES

Anderson, D. H. 1983. Compartmental Modeling and Tracer Kinetics. Springer-Verlag Berlin.

Ansari, A., J. Berendzen, S. F. Bowne, H. Frauenfelder, I. E. T. Iben, T. B. Sauke, E. Shyamsunder, and R. D. Young. 1985. Protein states and proteinquakes. Proc. Natl. Acad. Sci. USA. 82:5000–5004.

Birge, R. R. 1990. Photophysics and molecular electronic applications of the rhodopsins. Annu. Rev. Phys. Chem. 41:683–733.

Bogomolni, R. A., and J. L. Spudich. 1987. The photochemical reactions of bacterial sensory rhodopsin-I. Biophys. J. 52:1071–1075.

Braslavsky, S. E. 1990. Phytochrome. In Photochromism. Molecules and systems. H. Dürr and H. Bouas-Laurent, editors. Elsevier, Amsterdam. 738–754.

Eisfeld, W., C. Pusch, R. Diller, R. Lohrman, and M. Stockburger. 1993. Resonance raman and optical transient studies on the light-induced proton pump of bacteriorhodopsin reveal parallel photocycles. Biochemistry. 32: 7196–7215.

Fraser, R. D. B., and E. Suzuki. 1969. Resolution of overlapping bands: functions for simulating band shapes. Anal. Chem. 41:37–39.

Godfrey, K. 1983. Compartmental models and their application. Academic Press, London.

Golub, G. H., and R. J. LeVeque. 1979. Extensions and uses of the variable projection algorithm for solving nonlinear least squares problems. Proc. 1979 Army Numerical Analysis and Comput. Conf. ARO Report 79–3: 1–12.

Govindjee, R., B. Becher, and T. G. Ebry. 1978. The fluorescence from the chromophore of the purple membrane. Biophys. J. 22:67–77.

Henry, E. R., and J. Hofrichter. 1992. Singular value decomposition: application to analysis of experimental data. Methods Enzymol. 210:129–192.

Hessling, B., G. Souvignier, and K. Gerwert. 1993. A model-independent approach to assigning bacteriorhodopsin's intramolecular reactions to photocycle intermediates. Biophys. J. 65:1929–1941.

Hoff, W. D., S. L. S. Kwa, R. Van Grondelle, and K. J. Hellingwerf. 1992. Low temperature absorption and fluorescence spectroscopy of the yellow protein from Ectothiorhodospira halophila. Photochem. Photobiol. 56: 529–539.

Hoff, W. D., W. W. Sprenger, P. W. Postma, T. E. Meyer, M. Veenhuis, T. Leguijt, and K. J. Hellingwerf. 1994. The photoactive yellow protein from Ectothiorhodospira halophila as studied with a highly specific polyclonal antiserum: (intra)cellular localization, regulation of expression, and taxonomic distribution of cross-reacting proteins. J. Bacteriol. 176: 3920–3923.

Imhoff, J. F., and H. G. Trüper. 1977. Ectothiorhodospira halophila sp. nov., a new extremely halophilic phototrophic bacterium containing bacteriochlorophyll b. Arch. Microbiol. 114:115–121.

Kaufman, L. 1975. A variable projection method for solving separable nonlinear least squares problems. BIT 15:49–57.

Knutson, J. R., J. M. Beechem, and L. Brand. 1983. Simultaneous analysis of multiple fluorescence decay curves: a global approach. Chem. Phys. Lett. 102:501–507.

Lakowicz, J. R. 1983. Principles of fluorescence spectroscopy. Plenum Press, New York.

Lanyi, J. K. 1992. Proton transfer and energy coupling in the bacteriorhodopsin photocycle. J. Bioenerg. Biomembr. 24:169–179.

Lewis, A., J. P. Spoonhower, and G. J. Perreault. 1976. Observation of light emission from a rhodopsin. Nature. 260:675–678.

Lozier, R. H., A. Xie, J. Hofrichter, and G. M. Clore. 1992. Reversible steps in the bacteriorhodopsin photocycle. Proc. Natl. Acad. Sci. USA. 89: 3610–3614.

Malinowski, E. R. 1991. Factor analysis in chemistry. 2nd ed. Wiley, New York.

Mathies, R. A., S. W. Lin, J. B. Ames, and W. T. Pollard. 1991. From femtoseconds to biology: mechanism of bacteriorhodopsin's light-driven proton pump. Annu. Rev. Biophys. Chem. 20:491–518.

McRee, D. E., J. A. Tainer, T. E. Meyer, J. Van Beeumen, M. A. Cusanovich, and E. D. Getzoff. 1989. Crystallographic structure of a photoreceptor protein at 2.4 Å resolution. Proc. Natl. Acad. Sci. USA. 86: 6533–6537.

Meyer, T. E. 1985. Isolation and characterization of soluble cytochromes, ferredoxins and other chromophoric proteins from the halophilic phototrophic bacterium Ectothiorhodospira halophila. Biochim. Biophys. Acta. 806:175–183.

Meyer, T. E., M. A. Cusanovich, and G. Tollin. 1993. Transient proton uptake and release is associated with the photocycle of the photoactive yellow protein from the purple phototrophic bacterium Ectothiorhodospira halophila. Arch. Biochem. Biophys. 306:515–517.

Meyer, T. E., J. C. Fitch, R. G. Bartch, G. Tollin, and M. A. Cusanovich. 1990. Soluble cytochromes and a photoactive yellow protein isolated from the moderately halophilic purple phototrophic bacterium, Rhodospirillum salexigens. Biochim. Biophys. Acta. 1016:364–370.

Meyer, T. E., G. Tollin, T. P. Causgrove, P. Cheng, and R. E. Blankenship. 1991. Picosecond decay kinetics and quantum yield of fluorescence of the photoactive yellow protein from the halophilic purple phototrophic bacterium, Ectothiorhodospira halophila. Biophys. J. 59:988–991.

Meyer, T. E., G. Tollin, J. H. Hazzard, and M. A. Cusanovich. 1989. Photoactive yellow protein from the purple phototrophic bacterium, Ectothiorhodospira halophila. Biophys. J. 56:559–564.

Meyer, T. E., E. Yakali, M. A. Cusanovich, and G. Tollin. 1987. Properties of a water-soluble yellow protein isolated from a halophilic phototrophic bacterium that has photochemical activity analogous to sensory rhodopsin. Biochemistry. 26:418–423.

Miller, A., H. Leigeber, W. D. Hoff, and K. J. Hellingwerf. 1993. A light-dependent branching-reaction in the photocycle of the yellow protein from Ectothiorhodospira halophila. Biochim. Biophys. Acta. 1141:190–196.

Nagle, J. F. 1991. Solving complex photocycle kinetics. Theory and direct method. Biophys. J. 59:476–487.

Oesterhelt, D. and J. Tittor. 1989. Two pumps, one principle: light-driven ion transport in Halobacteria. TIBS 14:57–61.

Provencher, S. W. 1982. A constrained regularization method for inverting data represented by linear algebraic or integral equations. Comp. Phys. Comm. 27:213–227.

Provencher, S. W. and R. H. Vogel. 1980. Information loss with transform methods in system identification: a new set of transforms with high information content. Math. Biosci. 50:251–262.

Scurlock, R. D., C. H. Evans, S. E., Braslavsky, and K. Schaffner. 1993. A phytochrome phototransformation study using two-laser/two-color flash photolysis: analysis of the decay mechanism of I_{700}. Photochem. Photobiol. 58:106–115.

Sevilla, J. M., M. Dominguez, F. Garcia-Blanco, and M. Blazquez. 1989. Resolution of absorption spectra. Comput. Chem. 13:197–200.

Sprenger, W. W., W. D. Hoff, J. P. Armitage, and K. J. Hellingwerf. 1993. The Eubacterium Ectothiorhodospira halophila is negatively phototactic, with a wavelength dependence that fits the absorbance spectrum of the photoactive yellow protein. J. Bacteriol. 175:3096–3104.

Spudich, J. L. and R. A. Bogomolni. 1988. Sensory rhodopsins of halobacteria. *Annu. Rev. Biophys. Biophys. Chem.* 17:193–215.

Stavenga, D. G., J. Schwemer, and K. J. Hellingwerf. 1991. Visual pigments, bacterial rhodopsins and related retinoid-binding proteins. *In* Photoreceptor Evolution and Function. M. G. Holmes, editor. Academic Press, London. 261–349.

Van Beeumen, J., B. Devreese, S. Van Bun, W. D. Hoff, K. J. Hellingwerf, T. E. Meyer, D. E. McRee, and M. A. Cusanovich. 1993. The primary structure of a photoactive yellow protein from the phototrophic bacterium, *Ectothiorhodospira halophila*, with evidence for the mass and the binding site of the chromophore. *Prot. Sci.* 2:1114–1125.

Van Stokkum, I. H. M., A. M. Brouwer, H. J. van Ramesdonk, and T. Scherer. 1993. Multiresponse parameter estimation and compartmental analysis of time resolved fluorescence spectra. Application to conformational dynamics of charge-separated species in solution. *Proc. K. Ned. Akad. Wel. Ser. B. Phys. Sci.* 96:43–68.

Van Stokkum, I. H. M., T. Scherer, A. M. Brouwer, and J. W. Verhoeven. 1994. Conformational dynamics of flexibly and semirigidly bridged electron donor-acceptor systems as revealed by spectrotemporal parameterization of fluorescence. *J. Phys. Chem.* 98:852–866.

Váró, G. and J. K. Lanyi. 1991. Thermodynamics and energy coupling in the bacteriorhodopsin photocycle. *Biochemistry.* 30:5016–5022.

Weisberg, S. 1985. Applied Linear Regression. 2nd. ed. Wiley, New York.

Zimányi, L. and J. K. Lanyi. 1993. Deriving the intermediate spectra and photocycle kinetics from time-resolved difference spectra of bacteriorhodopsin. *Biophys. J.* 64:240–251.